Nano Research
https://doi.org/10.1007/s12274-017-1872-0
Research Article
ISSN 1998-0124
CN 11-5974/O4

Self-quenched gold nanoclusters for turn-on fluorescence imaging of intracellular glutathione

Cong Dai[1], Chengxiong Yang[1], and Xiuping Yan[1,2,3,4] (✉)

[1] *College of Chemistry, Research Center for Analytical Sciences, Tianjin Key Laboratory of Molecular Recognition and Biosensing, Nankai University, Tianjin 300071, China*
[2] *State Key Laboratory of Food Science and Technology, Jiangnan University, Wuxi 214122, China*
[3] *Institute of Analytical Food Safety, School of Food Science and Technology, Jiangnan University, Wuxi 214122, China*
[4] *Collaborative Innovation Center of Chemical Science and Engineering (Tianjin), 94 Weijin Road, Tianjin 300071, China*

Received: 4 September 2017
Revised: 27 September 2017
Accepted: 28 September 2017

KEYWORDS
self-quenching,
gold nanoclusters,
imaging,
intracellular glutathione

ABSTRACT

Activatable fluorescence nanoprobes with only one kind of nanomaterial that can act as both the energy donor and acceptor simultaneously are scarce, but highly desirable for biosensing and bioimaging. In the present study, we reveal the preparation of self-quenched gold nanoclusters as a simple fluorescent turn-on probe for imaging intracellular glutathione. The self-quenched gold nanoclusters are prepared via disulfide bond-induced aggregation of gold nanoclusters. Compared with monodisperse gold nanoclusters, the developed self-quenched gold nanoclusters exhibit weak emission at 735 nm with a 40-nm red shift and much lower quantum yield (0.69%). The prepared self-quenched gold nanoclusters also possess good sensitivity and selectivity for glutathione detection, and are applicable for fluorescent turn-on imaging of intracellular glutathione.

1 Introduction

Fluorescence turn-on nanoprobes with high signal to background ratios are of great importance in biosensing and bioimaging [1–22]. In general, fluorescence turn-on nanoprobes are composed of energy donors and acceptors. The donors can be many kinds of fluorescent nanomaterials, such as quantum dots [4–7], upconversion nanoparticles [8], persistent luminescence nanoparticles [9, 10], and noble metal nanoclusters [11–13, 16]. The acceptors are usually graphene oxide [12], single-walled carbon nanotubes [16], gold nanorods or nanoparticles [10, 13, 15], metal ions [9, 14, 17], and magnetic particles [18]. As such, most of the previous turn-on nanoprobes are complicated by the presence of two different components. Therefore, it is highly desirable to develop turn-on nanoprobes made with only one kind of nanomaterial that can act as both the donor and the acceptor simultaneously.

Noble metals, such as Au and Ag, nanoclusters have received significant attention because of their good fluorescence properties and low toxicity [23, 24].

Address correspondence to xpyan@nankai.edu.cn

Recently, great progress in the application of gold nanoclusters (AuNCs) and silver nanoclusters (AgNCs) has been made for biosensing and bioimaging [11–13, 16, 25–37]. In our previous work, we observed a significant red shift of AgNCs fluorescence caused by re-absorption caused by the aggregation of AgNCs [27]. Aggregated oligo-glutathione-AuNCs possess bright aggregation-induced enhanced fluorescence when confined in chitosan, poly(allylamine hydrochloride), or metal-organic frameworks [28–30]. Besides, quite a few fluorescent nanoprobes have been prepared based on the analyte-induced aggregation of noble-metal nanoclusters [31–37]. However, studies on re-dispersion after the aggregation of noble-metal nanoclusters and its application in biosensing and bioimaging are scarce.

In the present study, we report the fabrication of self-quenched AuNCs for fluorescent turn-on imaging of intracellular glutathione. The self-quenched AuNCs were prepared via disulfide bond-induced aggregation of AuNCs, and thus consist of AuNCs only as both the energy donor and acceptor. Glutathione, the most abundant intracellular small thiol-peptide, plays crucial roles in many physiological and pathological process, such as maintaining biological redox homeostasis in biological systems [17, 38–40]. Its levels are elevated in various human cancer tissues compared with normal tissues [41, 42]. Thus, it is of great importance to monitor the concentration of intracellular glutathione. In this work, we show the applicability of the self-quenched AuNCs for sensitive glutathione detection and fluorescence turn-on imaging of intracellular glutathione.

2 Experimental

2.1 Reagents

All reagents used were at least of analytical grade. Dimethyl sulfoxide (DMSO) was bought from Concord Technology (Tianjin, China). Glutathione (GSH), buthionine-sulfoximine (BSO), and formaldehyde were from Aladdin (Shanghai, China). Dithiobis (succinimidyl propionate) (DSP) was purchased from Tokyo Chemical Industry Co. (Shanghai, China). Phosphate-buffered saline (PBS) (10 mM, pH 7.4), bovine serum albumin (BSA), Dulbecco's modified Eagle's high glucose medium (DMEM), chloroauric acid ($HAuCl_4 \cdot 4H_2O$), fetal bovine serum, penicillin-streptomycin, 4′,6-diamidino-2-phenylindole (DAPI), and 3-(4,5-dimethyl-2-thiazolyl)-2,5-diphenyl-2-H-tetrazolium bromide (MTT) were purchased from Dingguo Biotechnology Co. (Beijing, China). Tyrosine (Tyr), homocysteine (Hcy), methionine (Met), histidine (His), tryptophan (Trp), alanine (Ala), serine (Ser), aspartic acid (Asp), and cysteine (Cys) were obtained from Newprobe Biotechnology Co. (Beijing, China). Ultrapure water was from Hangzhou Wahaha Group Co. (Hangzhou, China).

2.2 Instrumentation and characterization

The gold content was determined on an X series inductively coupled plasma mass spectrometer (ICP-MS) (Thermo Elemental, Altrincham, UK). Fourier transform infrared (FTIR) spectra in KBr were recorded on a Nicolet 6700 spectrometer (Thermo Fisher Scientific, USA). The transmission electron microscopy (TEM) images and the energy dispersive X-ray (EDX) analysis were carried out using a Tecnai G2 F20 transmission electron microscope (FEI, USA) with an accelerating voltage of 200 kV. The hydrodynamic size was determined on a Nano-ZS Zetasizer (Malvern, Malvern, UK). X-ray photoelectron spectroscopy (XPS) analysis was conducted on an Axis Ultra DLD spectrometer fitted with a monochromated Al Kα X-ray source ($h\nu$ = 1,486.6 eV), hybrid (magnetic/electrostatic) optics, and a multichannel plate, and delay line detector (Kratos Analytical Ltd., Manchester, UK). The absorption spectra were obtained on a UV-3600 ultraviolet-visual (UV-vis)-NIR spectrophotometer (Shimadzu, Japan). Fluorescence spectra were measured on an F-4500 spectrofluorometer (Hitachi, Japan). The MTT assay was performed on a Synergy HT plate reader (BioTek, USA). Microscopic images were collected on an FV1000S-IX81 fluorescent inverted microscope (Olympus, Japan).

2.3 Synthesis of self-quenched AuNCs (Sq-AuNCs)

BSA protected AuNCs (BSA-AuNCs) were prepared according to a typical method [43, 44]. The as-prepared BSA-AuNCs solution (5 mL) was mixed with 200 mg

of DSP in 15 mL of DMSO under ultrasonication for 30 min. The solution was then diluted with 60 mL of ultrapure water. After adjusting to pH 5 with diluted HCl, the crude precipitate was collected by centrifugation (9,000 rpm, 10 min) and washed with ultrapure water. Subsequently, the precipitate was re-dispersed in 40 mL of PBS. The transparent solution containing 0.64 mM gold was hereafter referred to Sq-AuNCs. In addition, a series of Sq-AuNCs with different aggregation levels were synthesized using different amounts of DSP. The quantum yield of Sq-AuNCs was measured in ultrapure water by a relative comparison method using the following Eq. (1) [45]

$$Q_{Sq} = Q_{BSA} \times (I_{Sq}/A_{Sq})/(I_{BSA}/A_{BSA}) \quad (1)$$

where Q, I, and A are the quantum yield, the integral area under the correction emission spectrum, and the absorbance at 520 nm, respectively, while Sq and BSA represent Sq-AuNCs and BSA-AuNCs, respectively.

2.4 Glutathione-activated fluorescence recovery assessment

A glutathione solution (0.25 M) was prepared with PBS, and adjusted to pH 7.4. A certain volume of the glutathione solution was added to 1 mL of 0.064 mM Sq-AuNCs solution under stirring at 37 ℃. Fluorescence spectra were recorded to evaluate the effect of time and the glutathione concentration on fluorescence recovery. The limit of detection (LOD) was calculated according to LOD = $3s/k$, where s and k are the standard deviations for 10 replicate detections of the blank and the slope of the calibration function, respectively.

2.5 Cell culture

A human hepatocarcinoma cell line (HepG-2), human breast cancer cell line (MCF-7), mouse oral squamous carcinoma cell line (SCC-7), and Balb/C mouse embryo fibroblasts cell line (Balb/3T3) (China Center for Type Culture Collection (CCTCC) (Wuhan, China)) were cultured in DMEM, which was supplemented with 10% fetal bovine serum and 1% penicillin-streptomycin. The cells were maintained in a humidified atmosphere of 5% CO_2 at 37 ℃ with the use of fresh DMEM every other day.

2.6 Cytotoxicity assay

HepG-2, MCF-7, SCC-7, or Balb/3T3 cells were seeded in 96-well plates (1×10^4 cells/well) for 12 h. The cultured cells were then incubated with the Sq-AuNCs in a concentration range of 0–200 μM. After 24 h of incubation, the viability of the cells was assessed using the MTT assay.

2.7 Turn-on fluorescence imaging of intracellular glutathione

HepG-2 cells were seeded in 24-well plates (5×10^4 cells/well) and incubated for 12 h. The seeded HepG-2 pretreated with 0.5 mM BSO (a good glutathione inhibitor [46]) for 20 min were used as the negative group, while the positive group was obtained from the negative group with a further 20-min incubation with 10 mM glutathione. The seeded HepG-2 without any pretreatments was used as the control group. The above three groups of cells were separately incubated with 0.2 mM Sq-AuNCs for 12 h, immobilized with formaldehyde (4%) for 30 min, and their nuclei were stained with 0.1 $mg \cdot mL^{-1}$ DAPI for 10 min. The cells were washed with PBS for subsequent fluorescence imaging with a cyan excitation source. The fluorescence imaging of intracellular glutathione in MCF-7, SCC-7, and Balb/3T3 were also accomplished in the same way to further verify the applicability of Sq-AuNCs for fluorescent turn-on imaging of intracellular glutathione. The cell lysate was obtained from 1×10^6 cells/mL solution after homogenization and ultrasonication. The Sq-AuNCs were mixed with the cell lysate. After a 6-h incubation at 37 ℃, fluorescence spectra were recorded to determine the glutathione concentration.

3 Results and discussion

3.1 Synthesis and characterization of Sq-AuNCs

The fabrication of the Sq-AuNCs and the principle for turn-on fluorescence imaging of intracellular glutathione are illustrated in Scheme 1. To obtain the

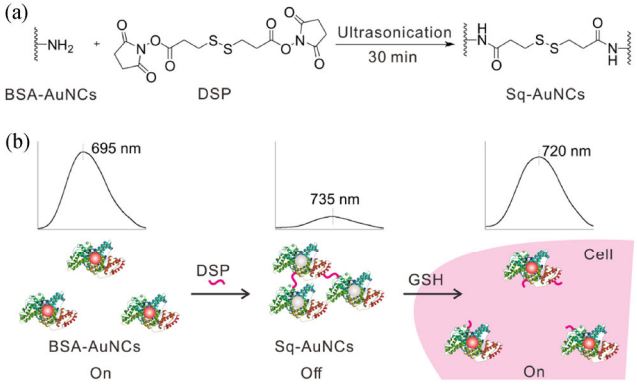

Scheme 1 (a) Route for the preparation of the self-quenched gold nanoclusters (Sq-AuNCs). (b) Principle of turn-on fluorescence imaging of intracellular glutathione.

Sq-AuNCs, BSA-AuNCs were bridged to each other via the condensation reaction between DSP and the amino group in the BSA-AuNCs (Scheme 1(a)).

The morphology and composition of the prepared Sq-AuNCs was characterized by FTIR, TEM, and EDX. The characteristic FTIR peaks of the disulfide bond in the Sq-AuNCs at 478 and 530 cm^{-1}, and the peak of the amide bond at 1,725 cm^{-1} demonstrated the successful interconnection of the BSA-AuNCs via DSP (Fig. 1(a)) [43, 47]. Besides, the presence of FTIR peaks of the BSA-AuNCs in the Sq-AuNCs indicated no obvious change of the structure of the BSA-AuNCs after aggregation (Fig. 1(a)).

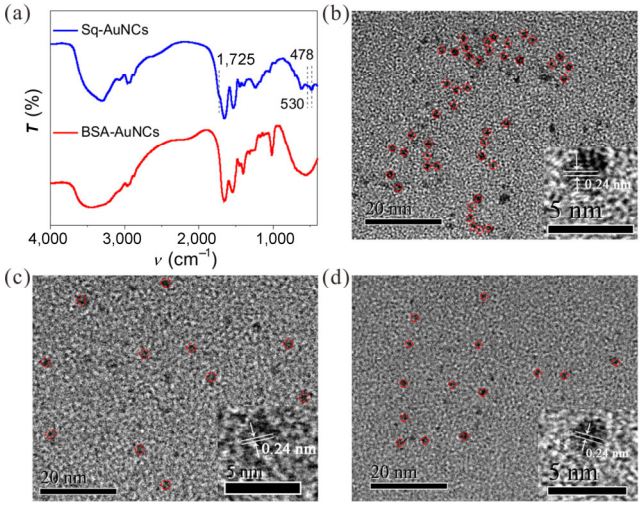

Figure 1 (a) FTIR spectra of bovine serum albumin-gold nanoclusters (BSA-AuNCs) (red) and self-quenched gold nanoclusters (Sq-AuNCs) (blue). TEM image of (b) Sq-AuNCs, (c) monodisperse BSA-AuNCs, and (d) glutathione-activated Sq-AuNCs. Inset: The lattice fringes of a single AuNC.

The TEM image of Sq-AuNCs shows the aggregation of AuNCs in comparison to that of monodisperse BSA-AuNCs (Fig. 1(b) cf. Fig. 1(c)). In addition, the diameter of a single AuNC in the Sq-AuNCs is 2.98 ± 0.07 nm, with a lattice spacing of 0.24 nm, which agrees with the d-spacing of the (111) crystal plane (Fig. 1(b)). Sq-AuNCs and BSA-AuNCs gave the same diameter and lattice fringe, also verifying the lack of changes to the BSA-AuNCs after aggregation (Fig. 1(c)) [48]. The EDX element analysis showed the presence of Au in BSA-AuNCs and Sq-AuNCs (Figs. S1(a) and S1(b) in the Electronic Supplementary Material (ESM)).

Sq-AuNCs showed a much larger hydrodynamic diameter (94.86 ± 3.26 nm) than that of BSA-AuNCs (13.64 ± 2.00 nm) (Fig. S2(a) in the ESM). The increase in the hydrodynamic diameter of Sq-AuNCs also demonstrated the aggregation of the BSA-AuNCs. Furthermore, the hydrodynamic diameter of a series of Sq-AuNCs synthesized with different amounts of DSP shows that the aggregation level increased with the amount of DSP (Fig. S2(b) in the ESM). In addition, the zeta potential of the Sq-AuNCs and BSA-AuNCs was −6.52 ± 0.44 and −7.38 ± 1.95 mV, indicating the almost constant zeta potential before and after the aggregation of the BSA-AuNCs (Fig. S3 in the ESM). The above results indicated the successful fabrication of the Sq-AuNCs.

3.2 Fluorescence properties of Sq-AuNCs

The prepared Sq-AuNCs gave the same absorption peaks at 520 nm as BSA-AuNCs, and exhibited a NIR emission at 735 nm, with a 40-nm red shift and much weaker intensity in comparison to the NIR emission of BSA-AuNCs (695 nm) (Fig. 2(a)). Moreover, there was no obvious change in the fluorescence spectra of the BSA-AuNCs after ultrasonication in the absence of DSP, which also verified the DSP-mediated aggregation (Fig. S4 in the ESM). Both the significant red shift and the decrease in fluorescence emission are different from the aggregation-induced emission of the oligo-glutathione-AuNCs confined in chitosan, poly(allylamine hydrochloride) and metal-organic frameworks [28–30]. The fluorescence mechanism of BSA-AuNCs is energy level transition without the

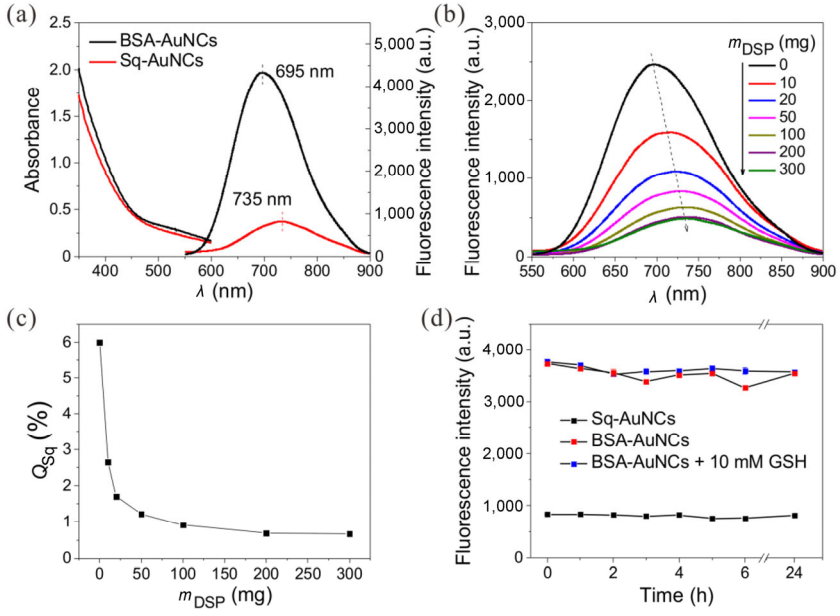

Figure 2 (a) UV-vis absorption spectra (left), fluorescence emission spectra (right) of bovine serum albumin-gold nanoclusters (BSA-AuNCs) (black), and the self-quenched gold nanoclusters (Sq-AuNCs) (red). (b) Fluorescence spectra of a series of Sq-AuNCs synthesized with different amounts of dithiobis(succinimidyl propionate) (DSP). (c) Effect of the amount of DSP on the quantum yield of Sq-AuNCs. (d) Colloidal stability of Sq-AuNCs (black), BSA-AuNCs (red), and BSA-AuNCs in the presence of 10 mM glutathione (blue). The concentration of Sq-AuNCs was 0.64 mM.

aggregation-induced enhancement. After the DSP-mediated crosslinking, the red tail of the absorption slightly absorbs the blue tail of the emission, which is termed re-absorption, leading to the significant fluorescence red shift and decrease in fluorescence emission [27, 49–51].

The contribution of the aggregation to the red shift and the decrease in fluorescence intensity was confirmed by measuring the fluorescence emission of a series of Sq-AuNCs with different aggregation levels (synthesized with different amounts of DSP) (Fig. 2(b)). The results showed that the emission of Sq-AuNCs was gradually red-shifted together with a decrease in fluorescence as the aggregation level increased.

The quantum yield of Sq-AuNCs (Q_{Sq}) was 0.69%, which was much smaller than that of BSA-AuNCs (6%) (Fig. 2(c)) [44]. Moreover, the Q_{Sq} decreased with the amount of DSP, further indicating the contribution of aggregation to the self-quenching (Fig. 2(c)). The Sq-AuNCs with quantum yield of 0.69% were used for the following experiments. In addition, both BSA-AuNCs and Sq-AuNCs also have good colloidal stability in PBS for at least 24 h, and BSA-AuNCs also showed good stability in the presence of 10 mM glutathione (Fig. 2(d)). The above results indicated the good stability of the Sq-AuNCs, together with much weaker emission than the BSA-AuNCs.

3.3 Glutathione-activated fluorescence recovery assessment

The mercapto group in glutathione can cleave the disulfide bond that bridges BSA-AuNCs in Sq-AuNCs; therefore, the aggregated AuNCs in the Sq-AuNCs would be re-dispersed in the presence of glutathione because of disaggregation. As a result, the NIR emission of the Sq-AuNCs in glutathione gradually blue-shifted in conjunction with an increase in fluorescence as time and the concentration of glutathione ([GSH]) increased (Figs. 3(a) and 3(b), and Fig. S5 in the ESM). In addition, no obvious increase in fluorescence was observed after a 6-h incubation. The quantum yield of glutathione-activated Sq-AuNCs finally increased to 5.08%.

The TEM image of glutathione-activated Sq-AuNCs directly shows the re-dispersion of AuNCs (Fig. 1(d) cf. Fig. 1(b)). Besides, the same lattice fringes, and

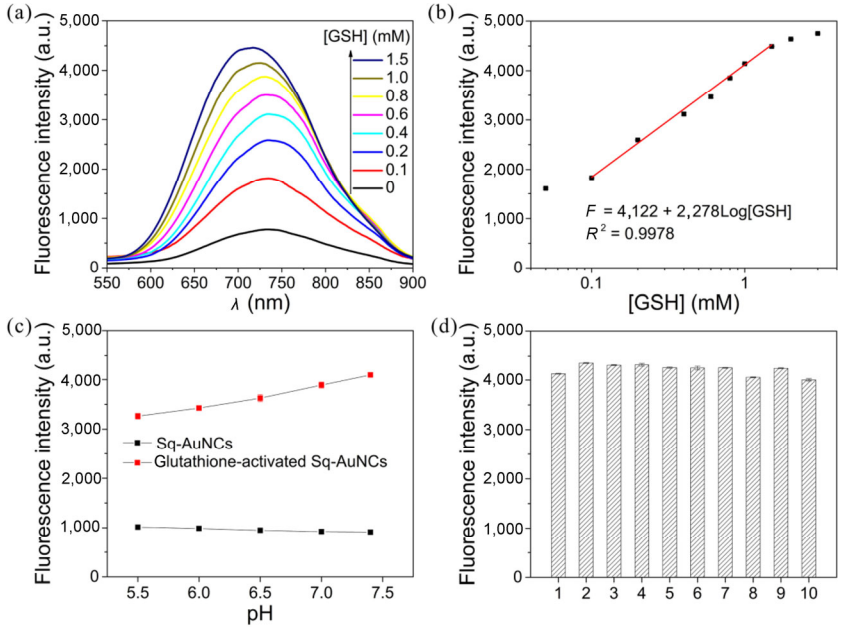

Figure 3 (a) Glutathione concentration-dependent fluorescence spectra of glutathione-activated self-quenched gold nanoclusters (Sq-AuNCs). (b) Plot of the fluorescence intensity of glutathione-activated Sq-AuNCs vs. the glutathione concentration. (c) pH dependent fluorescence intensity of the Sq-AuNCs (black) and the glutathione-activated Sq-AuNCs (red). (d) Effect of coexisting amino acids on the fluorescence intensity of glutathione-activated Sq-AuNCs. Note: 1, 1.5 mM glutathione; 2, 1.5 mM glutathione + 0.02 mM Cys; 3, 1.5 mM glutathione + 0.02 mM Hcy; 4, 1.5 mM glutathione + 1 mM Met; 5, 1.5 mM glutathione + 1 mM Ser; 6, 1.5 mM glutathione + 1 mM Trp; 7, 1.5 mM glutathione + 1 mM Ala; 8, 1.5 mM glutathione + 1 mM Asp; 9, 1.5 mM glutathione + 1 mM His; 10, 1.5 mM glutathione + 1 mM Tyr. The concentration of Sq-AuNCs was 0.064 mM.

similar EDX and FTIR spectra of glutathione-activated Sq-AuNCs indicated no obvious change in the structure of BSA-AuNCs after disaggregation (Fig. 1(d), Figs. S1(c) and S6 in the ESM). The hydrodynamic diameter of the glutathione-activated Sq-AuNCs was 36.4 ± 1.0 nm (Fig. S2(a) in the ESM), also indicating the re-dispersion of AuNCs. The zeta potential of Sq-AuNCs after the re-dispersion (−8.67 ± 0.69 mV) remained almost constant (Fig. S3 in the ESM). Moreover, similar fluorescence activation results (Fig. S7 in the ESM) and hydrodynamic diameters (35.3 ± 0.3 nm) were obtained with 1 mM dithiothreitol, a well-known reducing agent for disulfide bonds, verifying the re-dispersal mechanism comprising the breakage of disulfide bonds caused by the mercapto group in glutathione. Furthermore, no fluorescence recovery, but a slight intensity decrease of Sq-AuNCs was observed after incubation with trypsin (Fig. S8 in the ESM). The enzymatic degradation product of BSA might not protect the AuNCs very well, leading to a slight decrease in fluorescence.

The effect of pH on the fluorescence recovery of Sq-AuNCs with glutathione was also tested. In the physiologically relevant pH range, the NIR emission of Sq-AuNCs was almost constant (Fig. 3(c)). Even the fluorescence of glutathione-activated Sq-AuNCs exhibited a little decrease from pH 7.4 to 5.5 because of the decrease in the reducibility of the mercapto group [52]; the fluorescence recovery was still obvious (Fig. 3(c)).

We also examined the change in the fluorescence intensity of Sq-AuNCs with the concentration of glutathione at pH 7.4. The intensity of glutathione-activated AuNCs increased linearly with the denary logarithm of the glutathione concentration (Log[GSH]) in a concentration range of 0.1–1.5 mM, with a calibration function of F = 4,122 + 2,278Log[GSH] ([GSH] in mM, R^2 = 0.9978) (Fig. 3(b)). The limit of detection was 0.004 mM, which is enough to detect intracellular glutathione owing to the high intracellular glutathione concentration range (2–10 mM) [52, 53]. The relative standard deviation for 10 replicate

detections of 0.8 mM glutathione was 0.5%, showing highly precise glutathione detection.

To evaluate the selectivity of Sq-AuNCs for glutathione, the effect of certain typical coexisting amino acids on the emission intensity in the presence of 1.5 mM glutathione was investigated (Fig. 3(d)). The tolerant concentration of typical non-thiol-amino acids (His, Met, Ser, Trp, Tyr, Ala, and Asp) and thiol-amino acids (Hcy and Cys) was up to 1, 1, 1, 1, 1, 1, 1, 0.02, and 0.02 mM, respectively. Although the tolerant concentration of thiol-amino acids was 0.02 mM, this was still greater than their intracellular contents [53]. The above results demonstrated that the prepared Sq-AuNCs are promising as a glutathione sensor, with good sensitivity and selectivity.

3.4 Fluorescence turn-on imaging of intracellular glutathione

The cytotoxicity of the Sq-AuNCs was evaluated in Balb/3T3, HepG-2, MCF-7, and SCC-7 cells using the MTT assay (Fig. 4). No obvious cytotoxicity was observed up to 200 μM Sq-AuNCs.

To show the applicability of the prepared Sq-AuNCs for fluorescence turn-on imaging of intracellular glutathione, four kinds of cells were incubated with 0.2 mM Sq-AuNCs. Significant fluorescence in the cytoplasm of the control group of HepG-2 was observed after the incubation with Sq-AuNCs, while much lower fluorescence was observed in the negative group pretreated with the glutathione inhibitor BSO (Figs. 5(a) and 5(b)). In addition, subsequent incubation with glutathione in the positive group after pre-treatment with BSO resulted in strong fluorescence, demonstrating the glutathione-activation of Sq-AuNCs in HepG-2 cells (Fig. 5(c)). Furthermore, similar glutathione-activated fluorescence turn-on imaging results using Sq-AuNCs were obtained in MCF-7, SCC-7, and Balb/3T3 cells (Figs. S9–S11 in the ESM). The imaging results showed that fluorescence intensity in Balb/3T3 was weaker than that in the other cells. The amount of Au internalized in 1 × 10^6 HepG-2, MCF-7, SCC-7, and Balb/3T3 was 3.10, 3.40, 4.73, and 2.44 μg, respectively. The slightly lower amount of Au absorbed by the Balb/3T3 cells might be one of the reasons for the weaker fluorescence. Moreover, the lower intracellular glutathione concentration in Balb/3T3 cells could also account for their lower fluorescence intensity. The glutathione concentration in lysates from 1 × 10^6 cells/mL was determined by the Sq-AuNCs method (Table S1 in the ESM). The results showed that the cell lysates of HepG-2, MCF-7, and SCC-7 contained 1.00 ± 0.07, 1.10 ± 0.09, and 1.43 ± 0.10 mM glutathione, respectively. The glutathione concentration in Balb/3T3 lysate was 0.25 ± 0.01 mM, which was lower than those in the other three cell lines, verifying the fluorescence turn-on imaging results. The above results showed the applicability of the fabricated Sq-AuNCs for turn-on fluorescence imaging of intracellular glutathione.

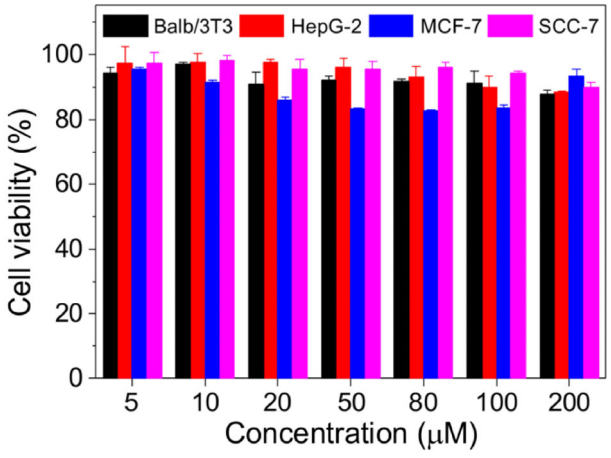

Figure 4 Cell viability of Balb/3T3 (black), HepG-2 (red), MCF-7 (blue), and SCC-7 (magenta) cells in the presence of self-quenched gold nanoclusters (Sq-AuNCs) in a concentration range of 0–200 μM. Error bars represent one standard deviation (n = 3).

4 Conclusions

In summary, we fabricated Sq-AuNCs via the aggregation of AuNCs bridged by disulfide bonds. The Sq-AuNCs consist only of AuNCs as both the energy donor and acceptor, and are promising as a simple glutathione-activatable fluorescence turn-on probe. The Sq-AuNCs possess a weak emission at 735 nm with a low quantum yield (0.69%), good stability, and low cytotoxicity. Furthermore, the Sq-AuNCs are promising as a sensitive and selective glutathione sensor, and are also applicable for turn-on fluorescence imaging of intracellular glutathione.

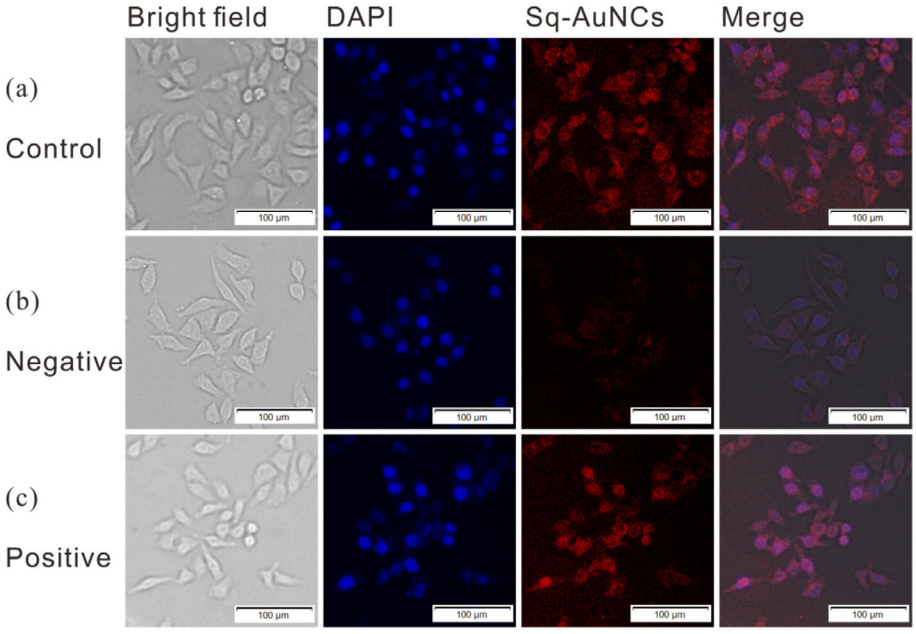

Figure 5 Fluorescence imaging of HepG-2 cells with 0.2 mM self-quenched gold nanoclusters (Sq-AuNCs). (a) The control group (without any pretreatment); (b) the negative group (pretreated with BSO); (c) the positive group (obtained from the negative group with further incubation of glutathione).

Acknowledgements

This work was supported by the National Natural Science Foundation of China (NSFC) (No. 21435001), the Fundamental Research Funds for Central Universities (No. JUSRP51714B), and the Open Funds of the State Key Laboratory of Electroanalytical Chemistry (No. SKLEAC201705).

Electronic Supplementary Material: Supplementary material (further details on the characterization of the Sq-AuNCs, glutathione-activated fluorescence recovery assay, and cell imaging) is available in the online version of this article at https://doi.org/10.1007/s12274-017-1872-0.

References

[1] Jun, M. E.; Roy, B.; Ahn, K. H. "Turn-on" fluorescent sensing with "reactive" probes. *Chem. Commun.* **2011**, *47*, 7583–7601.

[2] Kim, T.; Huh, Y. M.; Haam, S.; Lee, K. Activatable nanomaterials at the forefront of biomedical sciences. *J. Mater. Chem.* **2010**, *20*, 8194–8206.

[3] Kobayashi, H.; Ogawa, M.; Alford, R.; Choyke, P. L.; Urano, Y. New strategies for fluorescent probe design in medical diagnostic imaging. *Chem. Rev.* **2010**, *110*, 2620–2640.

[4] Wu, P.; Zhao, T.; Zhang, J. Y.; Wu, L.; Hou, X. D. Analyte-activable probe for protease based on cytochrome C-capped Mn: Zns quantum dots. *Anal. Chem.* **2014**, *86*, 10078–10083.

[5] Yan, X.; Song, Y.; Zhu, C. Z.; Song, J. H.; Du, D.; Su, X. G.; Lin, Y. H. Graphene quantum dot-MnO_2 nanosheet based optical sensing platform: A sensitive fluorescence "turn off-on" nanosensor for glutathione detection and intracellular imaging. *ACS Appl. Mater. Interfaces* **2016**, *8*, 21990–21996.

[6] Wang, Q.; Zhang, S. R.; Zhong, Y. G.; Yang, X. F.; Li, Z.; Li, H. Preparation of yellow-green-emissive carbon dots and their application in constructing a fluorescent turn-on nanoprobe for imaging of selenol in living cells. *Anal. Chem.* **2017**, *89*, 1734–1741.

[7] Gao, N.; Yang, W.; Nie, H. L.; Gong, Y. Q.; Jing, J.; Gao, L. J.; Zhang, X. L. Turn-on theranostic fluorescent nanoprobe by electrostatic self-assembly of carbon dots with doxorubicin for targeted cancer cell imaging, *in vivo* hyaluronidase analysis, and targeted drug delivery. *Biosens. Bioelectron.* **2017**, *96*, 300–307.

[8] Peng, J. J.; Xu, W.; Teoh, C. L.; Han, S. Y.; Kim, B.; Samanta, A.; Er, J. C.; Wang, L.; Yuan, L.; Liu, X. G. et al. High-efficiency *in vitro* and *in vivo* detection of Zn^{2+} by dye-assembled upconversion nanoparticles. *J. Am. Chem.*

Soc. **2015**, *137*, 2336–2342.

[9] Li, N.; Li, Y. H.; Han, Y. Y.; Pan, W.; Zhang, T. T.; Tang, B. A highly selective and instantaneous nanoprobe for detection and imaging of ascorbic acid in living cells and *in vivo*. *Anal. Chem.* **2014**, *86*, 3924–3930.

[10] Wu, B. Y.; Wang, H. F.; Chen, J. T.; Yan, X. P. Fluorescence resonance energy transfer inhibition assay for α-fetoprotein excreted during cancer cell growth using functionalized persistent luminescence nanoparticles. *J. Am. Chem. Soc.* **2011**, *133*, 686–688.

[11] Zhou, Y.; Zhou, T. S.; Zhang, M.; Shi, G. Y. A DNA-scaffolded silver nanocluster/Cu^{2+} ensemble as a turn-on fluorescent probe for histidine. *Analyst* **2014**, *139*, 3122–3126.

[12] Wang, Y.; Chen, J. T.; Yan, X. P. Fabrication of transferrin functionalized gold nanoclusters/graphene oxide nano-composite for turn-on near-infrared fluorescent bioimaging of cancer cells and small animals. *Anal. Chem.* **2013**, *85*, 2529–2535.

[13] Qin, L.; He, X. W.; Chen, L. X.; Zhang, Y. K. Turn-on fluorescent sensing of glutathione S-transferase at near-infrared region based on fret between gold nanoclusters and gold nanorods. *ACS Appl. Mater. Interfaces* **2015**, *7*, 5965–5971.

[14] Meng, H. M.; Zhang, X. B.; Yang, C.; Kuai, H. L.; Mao, G. J.; Gong, L.; Zhang, W. H.; Feng, S. L.; Chang, J. B. Efficient two-photon fluorescence nanoprobe for turn-on detection and imaging of ascorbic acid in living cells and tissues. *Anal. Chem.* **2016**, *88*, 6057–6063.

[15] Zhao, X.; Yang, C. X.; Chen, L. G.; Yan, X. P. Dual-stimuli responsive and reversibly activatable theranostic nanoprobe for precision tumor-targeting and fluorescence-guided photothermal therapy. *Nat. Commun.* **2017**, *8*, 14998.

[16] Jiang, H.; Xu, G.; Sun, Y. M.; Zheng, W. W.; Zhu, X. X.; Wang, B. J.; Zhang, X. J.; Wang, G. F. A "turn-on" silver nanocluster based fluorescent sensor for folate receptor detection and cancer cell imaging under visual analysis. *Chem. Commun.* **2015**, *51*, 11810–11813.

[17] Hu, Y.; Heo, C. H.; Kim, G.; Jun, E. J.; Yin, J.; Kim, H. M.; Yoon, J. One-photon and two-photon sensing of biothiols using a bispyrene-Cu(II) ensemble and its application to image GSH in the cells and tissues. *Anal. Chem.* **2015**, *87*, 3308–3313.

[18] Li, Y. R.; Liu, Q.; Hong, Z. Y.; Wang, H. F. Magnetic separation-assistant fluorescence resonance energy transfer inhibition for highly sensitive probing of nucleolin. *Anal. Chem.* **2015**, *87*, 12183–12189.

[19] Zhu, X. H.; Zhao, T. B.; Nie, Z.; Miao, Z.; Liu, Y.; Yao, S. Z. Nitrogen-doped carbon nanoparticle modulated turn-on fluorescent probes for histidine detection and its imaging in living cells. *Nanoscale* **2016**, *8*, 2205–2211.

[20] Zhuang, Y.; Huang, F. J.; Xu, Q.; Zhang, M. S.; Lou, X. D.; Xia, F. Facile, fast-responsive, and photostable imaging of telomerase activity in living cells with a fluorescence turn-on manner. *Anal. Chem.* **2016**, *88*, 3289–3294.

[21] Shi, W.; Ma, H. M. Rhodamine B thiolactone: A simple chemosensor for Hg^{2+} in aqueous media. *Chem. Commun.* **2008**, 1856–1858.

[22] Zhou, J.; Ma, H. M. Design principles of spectroscopic probes for biological applications. *Chem. Sci.* **2016**, *7*, 6309–6315.

[23] Lu, Y. Z.; Chen, W. Sub-nanometre sized metal clusters: From synthetic challenges to the unique property discoveries. *Chem. Soc. Rev.* **2012**, *41*, 3594–3623.

[24] Tao, Y.; Li, M. Q.; Ren, J. S.; Qu, X. G. Metal nanoclusters: Novel probes for diagnostic and therapeutic applications. *Chem. Soc. Rev.* **2015**, *44*, 8636–8663.

[25] Zhang, L. B.; Wang, E. K. Metal nanoclusters: New fluorescent probes for sensors and bioimaging. *Nanotoday* **2014**, *9*, 132–157.

[26] Shamsipur, M.; Molaabasi, F.; Hosseinkhani, S.; Rahmati, F. Detection of early stage apoptotic cells based on label-free cytochrome C assay using bioconjugated metal nanoclusters as fluorescent probes. *Anal. Chem.* **2016**, *88*, 2188–2197.

[27] Dai, C.; Yang, C. X.; Yan, X. P. Ratiometric fluorescent detection of phosphate in aqueous solution based on near infrared fluorescent silver nanoclusters/metal-organic shell composite. *Anal. Chem.* **2015**, *87*, 11455–11459.

[28] Yahia-Ammar, A.; Sierra, D.; Mérola, F.; Hildebrandt, N.; Le Guével, X. Self-assembled gold nanoclusters for bright fluorescence imaging and enhanced drug delivery. *ACS Nano* **2016**, *10*, 2591–2599.

[29] Goswami, N.; Lin, F. X.; Liu, Y. B.; Leong, D. T.; Xie, J. P. Highly luminescent thiolated gold nanoclusters impregnated in nanogel. *Chem. Mater.* **2016**, *28*, 4009–4016.

[30] Cao, F. F.; Ju, E. G.; Liu, C. Q.; Li, W.; Zhang, Y.; Dong, K.; Liu, Z.; Ren, J. S.; Qu, X. G. Encapsulation of aggregated gold nanoclusters into metal-organic frameworks for real-time monitoring of drug release. *Nanoscale* **2017**, *9*, 4128–4134.

[31] Zhang, N.; Si, Y. M.; Sun, Z. Z.; Chen, L. J.; Li, R.; Qiao, Y. C.; Wang, H. Rapid, selective, and ultrasensitive fluorimetric analysis of mercury and copper levels in blood using bimetallic gold-silver nanoclusters with "silver effect"-enhanced red fluorescence. *Anal. Chem.* **2014**, *86*, 11714–11721.

[32] Xu, N.; Zhu, Q.; Kong, X. Y.; Meng, L. A sensitive detection of Cr(VI) in wide pH range using polyethyleneimine protected silver nanoclusters. *Anal. Methods* **2016**, *8*, 5684–5689.

[33] Liang, S.; Kuang, Y. F.; Ma, F. F.; Chen, S.; Long, Y. F. A sensitive spectrofluorometric method for detection of berberine hydrochloride using Ag nanoclusters directed by natural fish sperm DNA. *Biosens. Bioelectron.* **2016**, *85*, 758–763.

[34] Guo, Y. H.; Tong, X. Y.; Ji, L. Y.; Wang, Z. L.; Wang, H. Y.; Hu, J. M.; Pei, R. J. Visual detection of Ca^{2+} based on aggregation-induced emission of Au(I)-Cys complexes with superb selectivity. *Chem. Commun.* **2015**, *51*, 596–598.

[35] Shu, T.; Su, L.; Wang, J. X.; Lu, X.; Liang, F.; Li, C. Z.; Zhang, X. J. Value of the debris of reduction sculpture: Thiol etching of Au nanoclusters for preparing water-soluble and aggregation-induced emission-active Au(I) complexes as phosphorescent copper ion sensor. *Anal. Chem.* **2016**, *88*, 6071–6077.

[36] Yang, X. M.; Yang, L.; Dou, Y.; Zhu, S. S. Synthesis of highly fluorescent lysine-stabilized Au nanoclusters for sensitive and selective detection of Cu^{2+} ion. *J. Mater. Chem. C* **2013**, *1*, 6748–6751.

[37] Lai, X. D.; Tan, L. S.; Deng, X. L.; Liu, J. B.; Li, A. Q.; Liu, J. Y.; Hu, J. Q. Coordinatively self-assembled luminescent gold nanoparticles: Fluorescence turn-on system for high-efficiency passive tumor imaging. *ACS Appl. Mater Interfaces* **2017**, *9*, 5118–5127.

[38] Yin, J.; Kwon, Y.; Kim, D.; Lee, D.; Kim, G.; Hu, Y.; Ryu, J. H.; Yoon, J. Preparation of a cyanine-based fluorescent probe for highly selective detection of glutathione and its use in living cells and tissues of mice. *Nat. Protoc.* **2015**, *10*, 1742–1754.

[39] Wang, Y. H.; Jiang, K.; Zhu, J. L.; Zhang, L.; Lin, H. W. A fret-based carbon dot-MnO_2 nanosheet architecture for glutathione sensing in human whole blood samples. *Chem. Commun.* **2015**, *51*, 12748–12751.

[40] He, L. W.; Xu, Q. Y.; Liu, Y.; Wei, H. P.; Tang, Y. H.; Lin, W. Y. Coumarin-based turn-on fluorescence probe for specific detection of glutathione over cysteine and homocysteine. *ACS Appl. Mater. Interfaces* **2015**, *7*, 12809–12813.

[41] Schnelldorfer, T.; Gansauge, S.; Gansauge, F.; Schlosser, S.; Beger, H. G.; Nussler, A. K. Glutathione depletion causes cell growth inhibition and enhanced apoptosis in pancreatic cancer cells. *Cancer* **2000**, *89*, 1440–1447.

[42] Huang, Z. Z.; Chen, C.; Zeng, Z.; Yang, H.; Oh, J.; Chen, L.; Lu, S. C. Mechanism and significance of increased glutathione level in human hepatocellular carcinoma and liver regeneration. *FASEB J* **2001**, *15*, 19–21.

[43] Sun, S. K.; Dong, L. X.; Cao, Y.; Sun, H. R.; Yan, X. P. Fabrication of multifunctional Gd_2O_3/Au hybrid nanoprobe via a one-step approach for near-infrared fluorescence and magnetic resonance multimodal imaging *in vivo*. *Anal. Chem.* **2013**, *85*, 8436–8441.

[44] Xie, J. P.; Zheng, Y. G.; Ying, J. Y. Protein-directed synthesis of highly fluorescent gold nanoclusters. *J. Am. Chem. Soc.* **2009**, *131*, 888–889.

[45] Adhikari, B.; Banerjee, A. Facile synthesis of water-soluble fluorescent silver nanoclusters and Hg^{II} sensing. *Chem. Mater.* **2010**, *22*, 4364–4371.

[46] Kumar, S. M.; Swaminathan, K.; Clemens, D. L.; Dey, A. GSH protects against oxidative stress and toxicity in VL-17A cells exposed to high glucose. *Eur. J. Nutr.* **2015**, *54*, 223–234.

[47] Nakamoto, K. *Infrared and Raman Spectra of Inorganic and Coordination Compounds*; 6th ed. John Wiley & Sons: New York, 2009.

[48] Zhao, P.; He, K. Y.; Han, Y. T.; Zhang, Z.; Yu, M. Z.; Wang, H. H.; Huang, Y.; Nie, Z.; Yao, S. Z. Near-infrared dual-emission quantum dots-gold nanoclusters nanohybrid via co-template synthesis for ratiometric fluorescent detection and bioimaging of ascorbic acid *in vitro* and *in vivo*. *Anal. Chem.* **2015**, *87*, 9998–10005.

[49] Mizusawa, K.; Ishida, Y.; Takaoka, Y.; Miyagawa, M.; Tsukiji, S.; Hamachi, I. Disassembly-driven turn-on fluorescent nanoprobes for selective protein detection. *J. Am. Chem. Soc.* **2010**, *132*, 7291–7293.

[50] Li, X.; Zhu, S. J.; Xu, B.; Ma, K.; Zhang, J. H.; Yang, B.; Tian, W. J. Self-assembled graphene quantum dots induced by cytochrome C: A novel biosensor for trypsin with remarkable fluorescence enhancement. *Nanoscale* **2013**, *5*, 7776–7779.

[51] Ho, L. C.; Wu, W. C.; Chang, C. Y.; Hsieh, H. H.; Lee, C. H.; Chang, H. T. Aptamer-conjugated polymeric nanoparticles for the detection of cancer cells through "turn-on" retro-self-quenched fluorescence. *Anal. Chem.* **2015**, *87*, 4925–4932.

[52] Santra, S.; Kaittanis, C.; Santiesteban, O. J.; Perez, J. M. Cell-specific, activatable, and theranostic prodrug for dual-targeted cancer imaging and therapy. *J. Am. Chem. Soc.* **2011**, *133*, 16680–16688.

[53] Feng, D.; Song, Y. C.; Shi, W.; Li, X. H.; Ma, H. M. Distinguishing folate-receptor-positive cells from folate-receptor-negative cells using a fluorescence off-on nanoprobe. *Anal. Chem.* **2013**, *85*, 6530–6535.